

# Improvement of Coarse-Grained Particle Method for Materials: Finite-Temperature and Inhomogeneity Effects

T. Nakamura<sup>1</sup>, R. Kobayashi<sup>1</sup>, and S. Ogata<sup>1</sup>

**Abstract:** The coarse-grained particle (CGP) method has been proposed to coarse-grain a crystalline system of atoms to meso-scale. In the method, virtual particles are distributed in the system, and the inter-particle interaction is calculated through the constrained statistical ensemble average of the atomic Hamiltonian at a given temperature. For simplicity, however, the harmonic approximation has been used for the inter-atomic interaction and hence anharmonicity at finite temperatures has been ignored. We improve the former CGP method to incorporate the anharmonicity of atomic system at finite temperatures into the inter-particle interaction. Also the divide-and-conquer strategy is applied to calculate the inter-particle interaction locally for an inhomogeneous system. Demonstrative simulation runs show that the improved CGP method describes properly both anharmonicity at finite temperatures and difference in local stiffness due to the point defect.

**Keywords:** coarse-graining, meso-scale method, anharmonicity, finite temperature, inhomogeneity, hybrid simulation

## 1 Introduction

The nanotechnology, which realizes the physical properties and functions that cannot be found in bulk materials by exploiting combinatory settings about nano-scaled structure and atomic arrangement, has long been recognized as the frontier of engineering research [Fendler (1998)]. Since countless number of the settings need be considered, computer simulation based on the atomistic description has been playing an important role to reduce developing costs and times [Nakano, Bachlechner, Branicio, Campbell, Ebbsjo, Kalia, Madhukar, Ogata, Omeltchenko, Rino, Shimojo, Walsh, and Vashishta (2000)]. If we focus on the mechanical properties of the micro-electro-mechanical-system (MEMS) [Gad-el-Hak (2001)], for instance, interesting phenomena to be simulated include its deformation, vibration, impact-wave propagation, and fracture [*e.g.*, Anderson (1995)]. Due to the complexity of

---

<sup>1</sup> Nagoya Inst. Tech., Nagoya, Japan and JST-CREST

the boundary condition the simulation of the MEMS should be performed for realistic shape with realistic size.

The molecular dynamics (MD) simulation method that utilizes the empirical potential has been applied to atomistic systems [*e.g.*, Allen and Tildesley (1987)], while the density-functional theory (DFT) or molecular orbital method to electronic systems [*e.g.*, Kakiras (2003)]. However, applying such a method to the whole of the MEMS is quite inefficient. When we simulate the dynamical failure of the MEMS, while the crack-tip region requires atomistic or electronic description, the surrounding region may be treated with a continuum method considering the smallness of the deformation. Motivated by this, the concurrent-type hybrid schemes have been proposed [Broughton, Abraham, Bernstein, and Kaxiras (1999); Ogata, Lidorikis, Shimojo, Nakano, Vashishta, and Kalia (2001); Lu and Kaxiras (2005)]. In the hybrid scheme, a simulation system is partitioned in real space to regions, and various simulation methods such as the electronic structure calculation, the classical MD method, and the continuum method, are applied appropriately to the regions. There have been attempts to hybridize the classical MD method and the DFT to obtain continuous force-field on ions at the interface of the regions [Daprich, Komáromi, Byun, Morokuma, and Frisch (1999); Ogata, Shimojo, Kalia, Nakano, and Vashishta (2002); Ogata, Abe, Ohba, and Kobayashi (2010); Ogata (2005)]. Also, for the atomistic-continuum interface, a number of literatures exist not only about the static structure [Mullins and Dokainish (1982); Smirnova, Zhigilei, and Garrison (1999)] but also about the algorithm to suppress artificial reflection wave from the interface [Liu, Karpov, Zhang, and Park (2004); Xu and Belytschko (2008); Kobayashi, Nakamura, and Ogata (2010)].

We consider that the meso-scale method that can be hybridized with the atomistic method for accurate simulation of a solid is not established well as explained below. A proper meso-scale method to be used in the hybrid scheme should have the following features: (i) It gives the same elastic moduli as the atomistic method does; (ii) It gives comparative deformation energy and phonon dispersion relation to the atomic ones for a wide range of wavenumber; (iii) It takes into account finite-temperature effects including thermal expansion; (iv) It is applicable to the situation of large deformation; (v) It is applicable to inhomogeneous systems. As for the top-down approach from macroscopic scale, the finite element (FE) method [*e.g.*, Cook and Plesh (1989)] or the quasi-continuum (QC) method [Tadmor, Ortiz, and Phillips (1996); Miller and Tadmor (2002); Curtin and Miller (2003)] has been used as a meso-scale method in the hybrid scheme. The FE method ignores both atomic degrees of freedom in the element and large deformation of crystalline structure of atoms. Substantial discrepancy exists in the stress-strain relation at nano scales. Therefore the FE method usually requires heuristic, careful arrange-

ment of the elements in the system. To summarize, the FE method does not have the features (ii), (iii), and (iv). The QC method is an extension of the FE method. In the QC method, the element energy is determined from the underlying atomic configuration that is interpolated from relating nodal configuration. It is difficult for the QC method to take into account the anharmonic, collective fluctuation of atoms including the thermal expansion at finite temperatures from the first principles. The QC method does not have the feature (iii).

As for the bottom-up approach from the atomic scale, the coarse-grained particle (CGP) method has been proposed as a meso-scale method for a crystalline solid [Rudd and Broughton (1998)]. A recursive coarse-graining procedure has been presented also [Kobayashi, Nakamura, and Ogata (2008)]. In the CGP method, virtual particles (or CGP's) are distributed in the system, and each particle represents a group of neighboring atoms with proper weights. The inter-particle interaction is calculated through the constrained statistical ensemble average of the atomic Hamiltonian at a given temperature. Therefore, at the same coarse-graining level, the CGP method generally gives higher accuracies than the QC method does. The harmonic approximation has been applied to the inter-atomic interaction under the PBC's for analytical calculation of the stiffness matrix between the CGP's. In the case, though the formulation of the CGP method uses the statistical ensemble average at a finite temperature, no anharmonic effects and therefore essentially no thermal effects have been included [Kobayashi, Nakamura, and Ogata (2008)]. Also the former CGP method cannot be used directly to inhomogeneous systems as surface and defect that contain thousands of atoms at least, since the calculation of the stiffness matrix for the CGP's requires the inverse calculation of the dynamics matrix of whole set of atoms in the corresponding systems. Therefore the former CGP method lacks the features (iii), (iv), and (iv).

In this paper, we will improve the former CGP method to incorporate the anharmonicity of atomic system at finite temperatures into the inter-particle interaction through a Monte Carlo sampling. Also the divide-and-conquer strategy will be applied to calculate the inter-particle interaction locally for an inhomogeneous system. Thereby the improved CGP method will have all the above-mentioned five features. About the anharmonicity at finite temperatures, Ref. [Rudd and Broughton (2005)] gave the perturbation expansion results that surpass the former harmonic results. However their results are quite complicated for numerical evaluation, and also cannot be applied to inhomogeneous systems. As will be demonstrated in a wave propagation simulation, the improved CGP method will incorporate successfully the anharmonicity at finite temperatures. Another application of the improved CGP method about the wave scattering by a point defect will demonstrate its usefulness for inhomogeneous systems.

Proceeding sections are organized as follows. In Sec. 2, the physical accuracy of the former CGP method will be clarified from various points of views. Remarkable features of the CGP method will be discussed. In Sec. 3, the proper form of the weight matrix that controls the quality of the method will be obtained. In Sec. 4, we will propose a novel approach to incorporate the anharmonicity and thermal effects into the inter-particle interaction. Demonstrative simulation runs will be performed in Sec. 5 to examine the accuracy of the improved CGP method. Summary and concluding remarks will be given in Sec. 6.

## 2 Physical Accuracy of Former CGP Method

We review briefly the CGP method in its original form [Rudd and Broughton (1998); Kobayashi, Nakamura, and Ogata (2008)], and analyze its accuracy for some physical properties. Let a crystalline system be composed of  $N_{\text{atom}}$  atoms. The Hamiltonian of the atomic system is composed of the kinetic and potential energies as

$$H_{\text{atom}} = \sum_i \sum_{\mu}^{N_{\text{atom}} \text{ axes}} \frac{p_{i\mu}^2}{2m_i} + V_{\text{atom}}(\{\mathbf{r}_i\}) \quad (1)$$

with the mass  $m_i$ , position  $\mathbf{r}_i$ , and momentum  $\mathbf{p}_i$ . The atoms are labeled with  $i, j, \dots$ ; Cartesian axes in  $d$  dimensional system are denoted with Greek letters. The system will be coarse-grained to the total of  $N_{\text{CGP}} (\ll N_{\text{atom}})$  CG particles that are distributed in it. The particles are labeled with  $I, J, \dots$ . Each particle represents a group of neighboring atoms, and the groups have some overlaps. The necessity of the overlap will be explained in Sec. 3. Denoting the atomic displacements by  $\mathbf{u}_i \equiv \mathbf{r}_i - \mathbf{r}_i^{(0)}$  and the particle ones by  $\mathbf{U}_I \equiv \mathbf{R}_I - \mathbf{R}_I^{(0)}$ , we introduce the relation using the weight matrix  $\mathbf{w}$  as

$$U_{I\mu} = \sum_i \sum_{\nu}^{N_{\text{atom}} \text{ axes}} w_{I\mu, i\nu} u_{i\nu} . \quad (2)$$

In practice, we consider that  $\mathbf{w}$  is non-zero only for the same Cartesian axes of the particle and atom, and is the same for the Cartesian axes. That is,  $w_{I\mu, i\nu} \equiv \hat{w}_{Ii} \delta_{\mu\nu}$  with the Kronecker's delta  $\delta_{\mu\nu}$ . Also  $\mathbf{w}$  is assumed to be independent of time. Since  $N_{\text{CGP}} \ll N_{\text{atom}}$ , the relation may be considered as a large-scale (or macroscopic) constraint to the atomic system.

We assume that the target system of atoms is close to the local statistical equilibrium at temperature  $T$  ( $\beta \equiv 1/k_B T$ ). For given sets  $\mathbf{U}$  and  $\dot{\mathbf{U}}$  of particle displace-

ments and their time-derivatives, respectively, the partition function is

$$Z_{\text{CGP}}(\mathbf{U}, \dot{\mathbf{U}}) = \left( \prod_i^{N_{\text{atom}}} \iint d\mathbf{u}_i d\mathbf{p}_i \right) \exp(-\beta H_{\text{atom}}) \Delta \dot{\Delta} \quad (3)$$

where

$$\Delta = \prod_I^{N_{\text{CGP axes}}} \prod_{\mu} \delta \left( U_{I\mu} - \sum_i^{N_{\text{atom axes}}} \sum_v w_{I\mu,iv} u_{iv} \right) \quad (4)$$

and

$$\dot{\Delta} = \prod_I^{N_{\text{CGP axes}}} \prod_{\mu} \delta \left( \dot{U}_{I\mu} - \sum_i^{N_{\text{atom axes}}} \sum_v w_{I\mu,iv} p_{iv} / m_i \right). \quad (5)$$

The total energy of the coarse-grained system is then obtained as

$$E_{\text{CGP}} = -\frac{\partial \ln Z_{\text{CGP}}}{\partial \beta} = \frac{d}{2\beta} (N_{\text{atom}} - N_{\text{CGP}}) + \frac{1}{2} \dot{\mathbf{U}}^T \mathbf{M} \dot{\mathbf{U}} + \langle V_{\text{atom}} \rangle_{\mathbf{U}=\mathbf{w}\mathbf{u}}. \quad (6)$$

Here

$$\mathbf{M} = (\mathbf{w}\mathbf{m}^{-1}\mathbf{w}^T)^{-1} \quad (7)$$

is the mass matrix with  $m_{i\mu,j\nu} = m_i \delta_{ij} \delta_{\mu\nu}$ , and therefore  $M_{I\mu,J\nu} = M_{IJ} \delta_{\mu\nu}$ . Superscript 'T' indicates the transpose operation. The notation  $\langle \dots \rangle_{\mathbf{U}=\mathbf{w}\mathbf{u}}$  means to perform the canonical ensemble average under the constraint  $\mathbf{U} = \mathbf{w}\mathbf{u}$ .

In the former papers, the harmonic approximation has been used for the potential energy of the atomic system, *i.e.*,

$$V_{\text{atom}} = \sum_{i,j}^{N_{\text{atom axes}}} \sum_{\mu,\nu} \frac{1}{2} u_{i\mu} D_{i\mu,j\nu} u_{j\nu} \quad (8)$$

with the dynamical matrix  $\mathbf{D}$ . We have thereby obtained

$$E_{\text{CGP}} = \frac{d}{\beta} (N_{\text{atom}} - N_{\text{CGP}}) + \frac{1}{2} \left( \dot{\mathbf{U}}^T \mathbf{M} \dot{\mathbf{U}} + \mathbf{U}^T \mathbf{K} \mathbf{U} \right) \quad (9)$$

with the stiffness matrix calculated analytically as

$$\mathbf{K} = (\mathbf{w}\mathbf{D}^{-1}\mathbf{w}^T)^{-1}. \quad (10)$$

Defining the momenta of particles as  $\mathbf{P} \equiv \partial E_{\text{CGP}} / \partial \dot{\mathbf{U}} = \mathbf{M}\dot{\mathbf{U}}$ , we have found the CGP Hamiltonian, which is independent of  $\beta$ , as

$$H_{\text{CGP}} = \frac{1}{2} (\mathbf{P}^T \mathbf{M}^{-1} \mathbf{P} + \mathbf{U}^T \mathbf{K} \mathbf{U}) . \quad (11)$$

Because of the harmonic approximation, the potential energy term in  $H_{\text{CGP}}$  corresponds to the minimum-energy of the atomic system under the constraint  $\mathbf{U} = \mathbf{w}\mathbf{u}$  [Kobayashi, Nakamura, and Ogata (2008)]. Considering the translational invariance of the potential energy, the potential energy term in  $H_{\text{CGP}}$  is rewritten as

$$V_{\text{CGP}} \equiv \frac{1}{2} \mathbf{U}^T \mathbf{K} \mathbf{U} = -\frac{1}{4} \sum_{I,J}^{N_{\text{CGP}} \text{ axes}} \sum_{\mu,\nu} (R_{IJ,\mu} - R_{IJ,\mu}^{(0)}) K_{I\mu,J\nu} (R_{IJ,\nu} - R_{IJ,\nu}^{(0)}) \quad (12)$$

with  $R_{IJ,\mu} \equiv R_{I\mu} - R_{J\mu}$  and  $R_{IJ,\mu}^{(0)} \equiv R_{I\mu}^{(0)} - R_{J\mu}^{(0)}$ . We note that Eq. (12) is not a simple harmonic formula. The  $K_{I\mu,J\nu}$  differs depending on both pairs of particles and Cartesian axes. Hence the shear deformation can be described also with Eq. (12).

The essential factor that controls the physical accuracy of  $H_{\text{CGP}}$  is the weight matrix,  $\mathbf{w}$ . In the former paper, to set  $\mathbf{w}$ , we have recalled the interpolation function (or shape function) in the FE method [Cook and Plesh (1989)]. In the FE method, the displacement of atom- $i$  due to that of neighboring node- $I$  is estimated by multiplying the interpolation function  $N_{I\mu,iv} \equiv \hat{N}_{Ii} \delta_{\mu\nu}$  to the nodal displacement: that is,  $\mathbf{u} = \mathbf{N}^T \mathbf{U}$ . Comparing  $\mathbf{U} = \mathbf{w}\mathbf{u}$  in the CGP method and  $\mathbf{u} = \mathbf{N}^T \mathbf{U}$  in the FE method, we have set  $\hat{\mathbf{w}} = \hat{\mathbf{w}}^{(0)} \equiv (\hat{\mathbf{N}} \hat{\mathbf{N}}^T)^{-1} \hat{\mathbf{N}}$ , which satisfies  $\hat{\mathbf{w}} \hat{\mathbf{N}}^T = \mathbf{1}$ . Essentially the same formula of  $\hat{\mathbf{w}}^{(0)}$  has been derived and used in Refs. [Tang (2008); To and Li (2005)] for the projection of the atomic displacement to a coarse-scale system. For simplicity, we have adopted the linear- $\hat{\mathbf{N}}$  for each particle, which means that the  $\hat{\mathbf{N}}$  assumes the maximum value of unity on a particle and decreases linearly to zero toward the nearest-neighbor particles. We here note that the matrix sizes of  $\hat{\mathbf{N}}$  and  $\hat{\mathbf{w}}$  are both  $N_{\text{CGP}} \times N_{\text{atom}}$ . In the CGP method atomic displacements ( $\mathbf{u}$ ) are not determined uniquely by a given particle displacements ( $\mathbf{U}$ ), which is the fundamental difference from the FE or QC method that uses  $\mathbf{u} = \mathbf{N}^T \mathbf{U}$ . The ensemble average is therefore performed for  $d \times (N_{\text{atom}} - N_{\text{CGP}})$  degrees of freedom.

We add parenthetically that the formula of  $\hat{\mathbf{w}}$  introduced above to satisfy  $\hat{\mathbf{w}} \hat{\mathbf{N}}^T = \mathbf{1}$  with the non-square matrix  $\hat{\mathbf{N}}$  is familiar in the DFT, for example, in the Mulliken population analyses to obtain the effective atomic charges from the valence wavefunctions [Sánchez-Portal, Artacho, and Soler (1996)]. In the analyses the key idea is to construct the dual orbitals from the non-orthogonal atomic orbital basis. We here apply the same idea to the present problem. For simplicity we consider a 1D system. Relating to  $\mathbf{u} = \mathbf{N}^T \mathbf{U}$ , we define  $|\phi_I\rangle_i$  as the displacement of atom- $i$  interpolated from a given displacement of particle- $I$ . We then define the dual of the

vector  $|\phi_I\rangle$  as  $|\phi^I\rangle \equiv \sum_J |\phi_J\rangle (S^{-1})_{JI}$  and  $\langle\phi^I| \equiv \sum_J (S^{-1})_{IJ} \langle\phi_J|$  with  $S_{IJ} = \langle\phi_I|\phi_J\rangle$ . We thereby find  $\langle\phi^I|\phi_J\rangle = \sum_K (S^{-1})_{IK} \langle\phi_K|\phi_J\rangle = \delta_{IJ}$ . Comparing  $\langle\phi^I|\phi_J\rangle = \delta_{IJ}$  and  $\sum_i w_{Ii} (N^T)_{iJ} = \delta_{IJ}$ , we find  $\mathbf{w} = (\mathbf{N}\mathbf{N}^T)^{-1}\mathbf{N}$ .

We now analyze the physical accuracy of the former CGP method explained above. To this end, we prepare a simple spring-bead system in 1D. In the system,  $N_{\text{atom}} = 550$  atoms are placed uniformly at  $r_i^{(0)} \equiv ia_{\text{atom}}$  with  $i = 1, 2, \dots, N_{\text{atom}}$  under the periodic boundary condition (PBC). The inter-atomic potential is  $V_{\text{atom}} \equiv \sum_{i=1}^{N_{\text{atom}}} (c/2) \times (u_{i+1} - u_i)^2$  with the spring constant  $c$ . For the situation with the coarse-graining ratio  $r_{\text{CG}} \equiv N_{\text{atom}}/N_{\text{CGP}}$ , the CG particles are introduced at  $R_I^{(0)} = Ia_{\text{CGP}} \equiv Ir_{\text{CG}}a_{\text{atom}}$  with  $I = 1, 2, \dots, N_{\text{CGP}}$ . We use the weight matrix

$$w_{Ii}^{(0)} = \sum_J (\mathbf{N}\mathbf{N}^T)^{-1}_{IJ} N_{Ji} \quad (13)$$

with the linear interpolation function

$$N_{Ii} = \begin{cases} 1-x & \text{with } x = \frac{r_i^{(0)} - R_I^{(0)}}{R_{I+1}^{(0)} - R_I^{(0)}}, \quad \text{for } R_I^{(0)} \leq r_i^{(0)} \leq R_{I+1}^{(0)} \\ 1-x & \text{with } x = \frac{R_I^{(0)} - r_i^{(0)}}{R_I^{(0)} - R_{I-1}^{(0)}}, \quad \text{for } R_{I-1}^{(0)} < r_i^{(0)} < R_I^{(0)} \\ 0, & \text{otherwise.} \end{cases} \quad (14)$$

The  $N_{Ii}$  and  $w_{Ii}^{(0)}$  for  $r_{\text{CG}} = 10$  as functions of  $r = r_i^{(0)} - R_I^{(0)}$  are shown in Figs. 1(a) and 1(b), respectively. Note that  $w_{Ii}^{(0)}$  has both positive and negative regions, its importance will be explained later.

We compare the elastic constant, the phonon dispersion relation, and the deformation energies of the CGP system with that of the atomic system. In the former papers [Rudd and Broughton (1998); Kobayashi, Nakamura, and Ogata (2008)], only the elastic constant and phonon dispersion relation were considered. Though the elastic constant is directly related to the deformation energy at zero wavenumber limit, we consider that the wavenumber-dependence of the deformation energy needs be analyzed also when we apply the CGP method to real problems. Two cases are considered:  $r_{\text{CG}} = 2$  and 10. Firstly, we find that the elastic constant agrees perfectly well with that of the atomic one for both  $r_{\text{CG}}$ . Secondary, the phonon dispersion relation at the wavenumber range, except near the Brillouin zone-boundary  $\pi/a_{\text{CGP}}$ , agrees well with that of the atomic one for both  $r_{\text{CG}}$ . Figure 2(a) depicts the phonon dispersion relation for  $r_{\text{CG}} = 10$  by the crosses. The maximum wavenumber of the CGP system is  $1/r_{\text{CG}}$  times of that of the atomic system. The flattening behavior of the dispersion relation at around the boundary, observed in Fig. 2(a), is a consequence of the CGP periodicity and is inevitable. While both  $\mathbf{K}$  and  $\mathbf{M}$  change by the optimization of  $\mathbf{w}$  to be performed in Sec. 3, the phonon

frequency changes little as seen in Fig. 2(a) because it is related to a kind of ratio of  $\mathbf{K}$  to  $\mathbf{M}$ .

Thirdly, to analyze the deformation energy  $\Delta E$  at various wavenumbers, we apply the same deformation field in the Gaussian-form:

$$u_i \equiv A \exp \left( -\frac{(r_i^{(0)} - l^{(0)})^2}{\alpha^2} \right) \quad (15)$$

and

$$U_I \equiv A \exp \left( -\frac{(R_I^{(0)} - l^{(0)})^2}{\alpha^2} \right) \quad (16)$$

for the atomic and CGP systems, respectively, with  $A = 0.01a_{\text{atom}}$ . Here  $\alpha$  measures the width of the deformation peak centered at  $r = l^{(0)}$ . Figure 3(a) compares  $\Delta E$  of the CGP system for  $r_{\text{CG}} = 10$  and that of the atomic system. The minimum of  $\alpha$  plotted in Fig. 3(a) corresponds to the smallest possible value where the dependence of the CGP-deformation energy on the choice of  $l^{(0)}$  is negligible. We observe in Fig. 3(a) that: (i) The CGP-deformation energy at  $\alpha > 4a_{\text{CGP}}$  agrees reasonably well with the atomic one; (ii) the CGP-deformation energy at  $\alpha < 4a_{\text{CGP}}$  is underestimated substantially. Less substantial underestimation at small  $\alpha$  is observed for a smaller  $r_{\text{CG}}$ . Such an underestimation of the deformation energy in the CGP method has not been pointed out before.

The reason why the deformation energy at a large wavenumber (*i.e.*, small  $\alpha$ ) is underestimated is the following. As explained in a former paragraph, the potential energy of the CGP system corresponds to the minimum potential-energy of the atomic system in the harmonic approximation under the constraint  $\mathbf{U} = \mathbf{w}\mathbf{u}$ . Therefore, when a deformation field is applied to the CG particles through  $\mathbf{U}$ , the corresponding potential energy of the CGP system is always lower than that of the atomic system where the same deformation field is applied to all the atoms through  $\mathbf{u}$ . We stress that no such an underestimation is observed in the phonon dispersion relation since the wavenumber dependence of the mass matrix acts to compensate the underestimation of the deformation energy in the CGP method.

### 3 Proper Form of Weight Matrix

We require that the proper weight matrix in the CGP method should reproduce all the three quantities: the elastic moduli, the phonon dispersion relation, and the deformation energy. In this section we start with explaining the conditions for the weight matrix to satisfy, and then search for proper form of the weight matrix. Suppose an atomic system of finite size and its coarse-grained system to derive the

conditions of the weight matrix as follows.

**Condition 1:** Imagine that both atomic and CGP systems are displaced uniformly by the same amount:  $U_{I\mu} = u_{i\mu} = \text{constant}$  for all  $I$  and  $i$ . Since  $U_{I\mu} = \sum_i^{N_{\text{atom}}} \hat{w}_{Ii} u_{i\mu}$ , we find a sum rule for all  $I$

$$\sum_i^{N_{\text{atom}}} \hat{w}_{Ii} = 1. \quad (17)$$

**Condition 2:** Imagine that the same total amount of force is applied uniformly to both atomic and CGP systems. Both systems should move at the same acceleration without deformation. The equation of motion is  $(d/dt)(\partial \hat{\mathbf{U}}^T \mathbf{M} \hat{\mathbf{U}} / 2 \partial \hat{U}_{I\mu}) = \sum_J M_{IJ} \ddot{U}_{J\mu} = F_{I\mu}$  for the CGP system, while it is  $m_i \ddot{u}_{i\mu} = f_{i\mu}$  for the atomic system. Since  $\ddot{U}_{I\mu} = \ddot{u}_{i\mu} = \text{constant}$  for all  $I$  and  $i$ , and  $\sum_I F_{I\mu} = \sum_i f_{i\mu}$  by assumption, we find  $\sum_{I,J} M_{IJ} = \sum_i m_i$ . It means the conservation of total mass in the coarse-graining procedure. In the case of an atomic system with a single species,

$$\sum_{I,J} M_{IJ} = \sum_{I,J} (\hat{\mathbf{w}} m^{-1} \hat{\mathbf{w}}^T)^{-1} = m \sum_{I,J} (\hat{\mathbf{w}} \hat{\mathbf{w}}^T)^{-1} \quad (18)$$

Therefore we find

$$\sum_{I,J} [(\hat{\mathbf{w}} \hat{\mathbf{w}}^T)^{-1}]_{IJ} = N_{\text{atom}}. \quad (19)$$

The necessity of this condition has not been pointed out before.

In the remainder of this section, we will search for the proper weight-matrix for better physical accuracy of the CGP method under the conditions 1 and 2. We call the part of the weight matrix relating to a given CGP the weight function. For efficient search, we here examine the existing range of the weight function for each particle. Imagine that only a single particle is displaced. Then the range of those atoms that are displaced relatedly should extend beyond the halfway to the nearest neighbor particle. It is because the uniform displacement of the atomic system should be related to the situation of addition of the displacement for each particle in the CGP system. From that, we consider that the weight function for a given particle should extend also, at least, to the nearest neighbor particles. It means that the weight function for each particle should overlap with that for its surrounding particles. Also we require that the weight function for each particle should not be very long-ranged, in order for the CGP method to be able to describe various deformation shapes of the target system. The  $\hat{\mathbf{w}}^{(0)} = (\hat{\mathbf{N}} \hat{\mathbf{N}}^T)^{-1} \hat{\mathbf{N}}$  with the linear- $\hat{\mathbf{N}}$  explained in Sec. 2, in fact, satisfies both conditions 1 and 2. In the bead-spring system in 1D, the magnitude of  $\hat{\mathbf{w}}^{(0)}$  for a given particle is quite small at and beyond

the third nearest neighbor particle. We therefore set the existing range of the weight function for each particle within the fourth nearest neighbor particle.

It is remarkable that the matrix  $\hat{\mathbf{w}}^{(0)}$  with the linear- $\hat{\mathbf{N}}$  has both positive and negative elements. In this connection, we state that any weight-matrix with positive elements only, cannot satisfy both conditions 1 and 2 at the same time. Also we stress that the existence of both positive and negative elements in the weight matrix is required to satisfy the condition  $U_{I\mu} = \sum_i^{N_{\text{atom}}} \hat{w}_{Ii} u_{i\mu}$  in the situation where only a single particle is displaced to some direction (*i.e.*,  $U_{1\mu} > 0$  and  $U_{2\mu} = U_{3\mu} = \dots = U_{N_{\text{CGP}\mu}} = 0$ ) in the CGP system and its neighboring atoms are displaced correspondingly to the same direction (*i.e.*,  $u_{i\mu} \geq 0$  for all  $i$ ) in the atomic system.

In the search for proper weight-matrix for accurate description of the bead-spring system in 1D, we start by modifying  $\mathbf{w}^{(0)}$  under the conditions 1 and 2. Considering that the deformation of the CGP system is underestimated (see, Sec. 2), we should decrease the magnitude of  $\mathbf{w}$  to increase  $\mathbf{u}$  from the relation  $\mathbf{U} = \mathbf{w}\mathbf{u}$  for a given  $\mathbf{U}$ . We require that the matrix  $\mathbf{w}$  is composed of the equivalent weight-functions for all the particles relating to the homogeneity of the target system. The optimization algorithm for  $\mathbf{w}$  is the following:

**Step 1:** Set the cutoff distance  $r_c$  for  $w_{Ii}$  around  $3 \sim 4a_{\text{CGP}}$ .

**Step 2:** Add a constant to those  $w_{Ii}$  for atom- $i$  located within  $r_c$  from particle- $I$  so that  $w_{Ii} = 0$  at  $r_c$ . Also set  $w_{Ii} = 0$  for the atoms outside.

**Step 3:** Scale all  $w_{Ii}$  by the same factor to satisfy the condition 1 mentioned above. We find the condition 2 always satisfied with this scaling.

**Step 4:** Analyze the accuracies of physical quantities. If it is unsatisfactory, return to Step 1 for a different  $r_c$ .

We observe that the smaller the  $r_c$  the larger the central peak of  $w_{Ii}$ . In the case of  $r_{\text{CG}} = 10$ , we find with  $r_c = 3.40a_{\text{CGP}}$  that the deformation energy,  $\Delta E$ , with the optimized  $\mathbf{w}$  for various  $\alpha$  becomes quite close to the atomic one as depicted in Fig. 3(a). By the optimization, the elastic constant and phonon dispersion relation change negligibly as shown in Fig. 2(a). The optimized  $\mathbf{w}$  is plotted in Fig. 1(b). Despite the apparent discontinuity in the derivative of  $w_{Ii}$  with respect to  $r$ , various physical properties are reproduced quite accurately, which is a consequence of the ensemble average of atomic configurations inherent in the CGP method.

In the optimization of the weight matrix mentioned above, we have started from  $\mathbf{w}^{(0)} = (\mathbf{N}\mathbf{N}^T)^{-1}\mathbf{N}$  with the linear- $\mathbf{N}$ , and have modified it to reproduce the physical quantities accurately. Since various forms of the interpolation function have been used successfully in the FE method, it may be interesting to re-start the optimization with non-linear- $\mathbf{N}$ . The Hermitian interpolation that uses both nodal displacements and their derivatives is well known. Referring to the simplest Hermitian interpolation function [Cook and Plesh (1989)], we set the non-linear interpolation

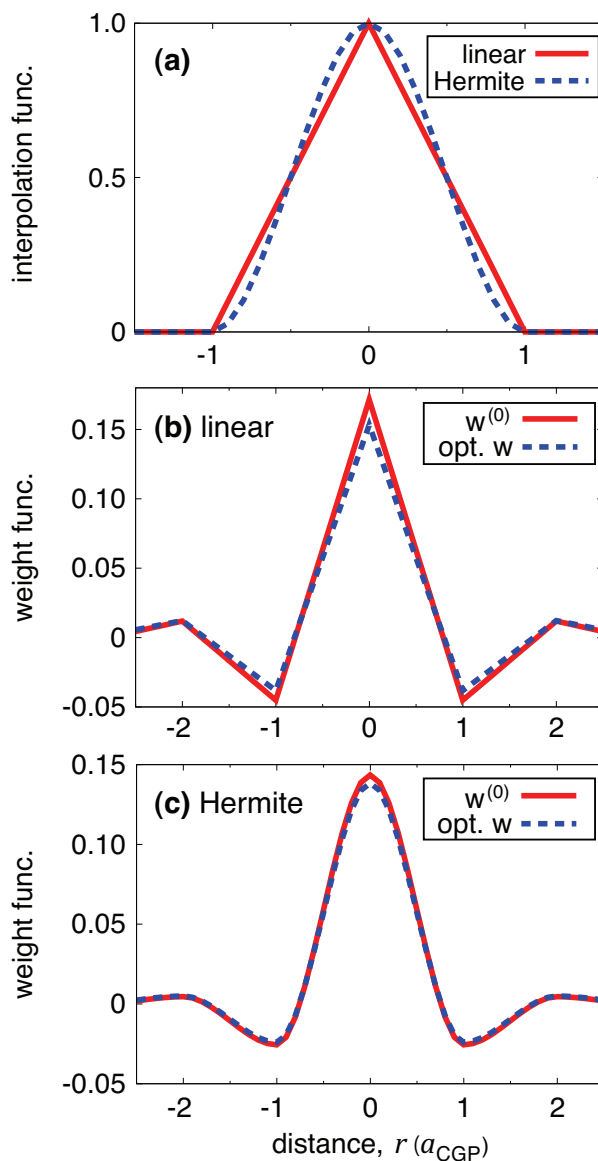


Figure 1: The interpolation function ( $\mathbf{N}$ ) and the weight function ( $\mathbf{w}$ ) of the spring-bead system in 1D with  $r_{CG} = 10$ . (a) The linear- $\mathbf{N}$  and Hermite- $\mathbf{N}$  as functions of the distance from a given CGP. (b) The  $\mathbf{w}^{(0)} = (\mathbf{N}\mathbf{N}^T)^{-1}\mathbf{N}$  with the linear- $\mathbf{N}$  and the optimized  $\mathbf{w}$  starting from  $\mathbf{w}^{(0)}$ . (c) The same as (b) but with the Hermite- $\mathbf{N}$ .

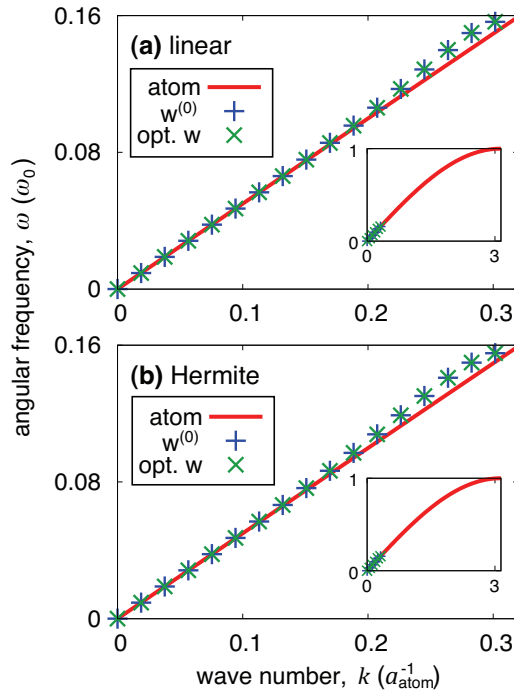


Figure 2: Comparison of the phonon dispersion relation of the spring-bead system in 1D between the CGP system with  $r_{\text{CG}} = 10$  and the atomic (spring-bead) system. (a) Using  $\mathbf{w}^{(0)} = (\mathbf{N}\mathbf{N}^T)^{-1}\mathbf{N}$  with the linear- $\mathbf{N}$  and the optimized  $\mathbf{w}$  starting from  $\mathbf{w}^{(0)}$ . (b) The same as (a) but with the Hermitian- $\mathbf{N}$ . The  $\omega_0 = 2\sqrt{c/m}$  is the maximum angular frequency. The insets depict the dispersion relations in the Brillouin zone.

function for the present purpose as

$$N_{Ii} = \begin{cases} 1 - 3x^2 + 2x^3 & \text{with } x = \frac{r_i^{(0)} - R_I^{(0)}}{R_{I+1}^{(0)} - R_I^{(0)}}, & \text{for } R_I^{(0)} \leq r_i^{(0)} \leq R_{I+1}^{(0)} \\ 1 - 3x^2 + 2x^3 & \text{with } x = \frac{R_I^{(0)} - r_i^{(0)}}{R_I^{(0)} - R_{I-1}^{(0)}}, & \text{for } R_{I-1}^{(0)} < r_i^{(0)} < R_I^{(0)} \\ 0, & \text{otherwise.} \end{cases} \quad (20)$$

Starting with the initial  $\mathbf{w}^{(0)} = (\mathbf{N}\mathbf{N}^T)^{-1}\mathbf{N}$ , we optimize  $\mathbf{w}$  in the same way as in the case of the linear- $\mathbf{N}$ , as depicted in Fig. 1(c) for  $r_{\text{CG}} = 10$ . The optimized results for the phonon dispersion relation and deformation energy are depicted in Figs. 2(b) and 3(b), respectively, for  $r_{\text{CG}} = 10$ . Though the deviation of the phonon dispersion

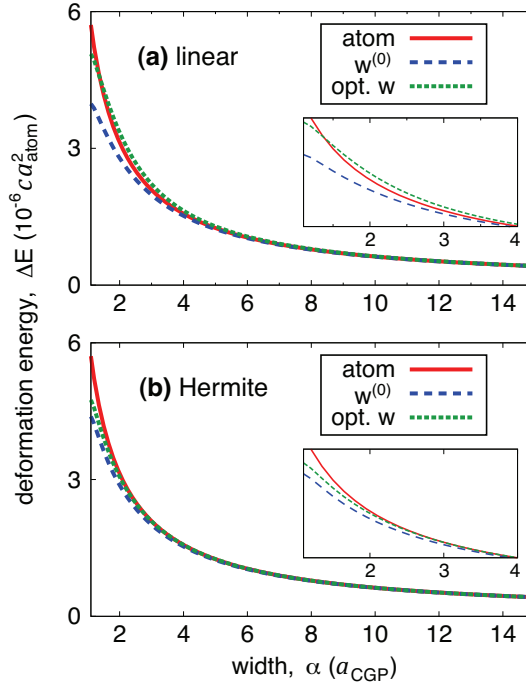


Figure 3: Comparison of the deformation energy ( $\Delta E$ ) of the spring-bead system in 1D between the CGP system with  $r_{\text{CG}} = 10$  and the atomic (spring-bead) system. The  $\alpha$  is the width of the deformation peak. (a) Using  $\mathbf{w}^{(0)} = (\mathbf{N}\mathbf{N}^T)^{-1}\mathbf{N}$  with the linear- $\mathbf{N}$  and the optimized  $\mathbf{w}$  starting from  $\mathbf{w}^{(0)}$ . (b) The same as (a) but with the Hermitian- $\mathbf{N}$ . The insets depict the zoom-up views.

relation from the atomic one is slightly larger at relatively large wavenumbers as compared to the case of the linear- $\mathbf{N}$ , the deformation energy compares quite well with the case of the linear- $\mathbf{N}$ .

We perform similar analyses also for the systems with other inter-atomic potentials such as the Lennard-Jones (LJ) potential [*e.g.*, Allen and Tildesley (1987)], to find similar increased accuracy by the optimization. We may conclude for 1D systems that the optimization of  $\mathbf{w}$ , starting with  $\mathbf{w}^{(0)} = (\mathbf{N}\mathbf{N}^T)^{-1}\mathbf{N}$  and either linear- or non-linear- $\mathbf{N}$ , gives quite accurate description not only for the elastic constant and phonon dispersion relation but also for the deformation energy.

We now apply the optimization procedure for the weight matrix to a 3D system. We consider the fcc-crystalline, cubic system of Al with  $N_{\text{atom}} = 320,000$  at the

ground state under the PBC's interacting with the embedded-atom method (EAM) potential [Finnis and Sinclair (1984); Streitz and Mintmire (1994)]. To coarse-grain the system at  $r_{CG} = 4$ , a particle is set at the center of each fcc unit of side-length  $a_{fcc}=4.01\text{\AA}$ . As for the weight matrix, we use either  $\hat{\mathbf{w}}^{(0)} = (\hat{\mathbf{N}}\hat{\mathbf{N}}^T)^{-1}\hat{\mathbf{N}}$  with the linear- $\hat{\mathbf{N}}$  or the modified  $\hat{\mathbf{w}}$  that reproduces the deformation energy as will be explained in the proceeding paragraph. Since the calculation of the stiffness matrix,  $\mathbf{K} = (\mathbf{w}\mathbf{D}^{-1}\mathbf{w}^T)^{-1}$ , involves the inverse calculation of the dynamical matrix,  $\mathbf{D}$ , of the atomic system, the direct calculation of  $\mathbf{K}$  for the total system is impractical. We therefore take the divide-and-conquer strategy and introduce temporarily a small cubic system of 500 atoms under the PBC's to calculate  $\mathbf{K}$  for  $N_{CGP} = 5 \times 5 \times 5$ , which means to introduce the truncation to the inter-particle interaction. The  $\mathbf{K}$  calculated thereby is then used extensively to all the particles considering the translational invariance of the fcc-crystalline system.

To calculate the deformation energy of the Al crystal, we apply the same Gaussian-form deformation field in  $x$ -direction, Eqs. (15) and (16), to both atomic and CGP systems. With  $\hat{\mathbf{w}}^{(0)}$ , we find 17–20% lower deformation energy at  $\alpha = 20.5 \sim 41.0\text{\AA}$  than the atomic one. The modified  $\hat{\mathbf{w}}$  reproduces the deformation energy quite accurately within 1% difference. As for the phonon dispersion relation, similarly to the 1D case, it is insensitive to the weight matrix and agrees well with the atomic one, except at around the Brillouin-zone boundary [Ashcroft and Mermin (1976)].

Unfortunately, the shear moduli [Ashcroft and Mermin (1976)] of the 3D-Al crystal calculated with the modified  $\hat{\mathbf{w}}$  are less accurate as compared to that with the  $\hat{\mathbf{w}}^{(0)}$ . The elastic moduli for the CGP system are  $(C_{11}, C_{12}, C_{44}) = (9.20\text{GPa}, 4.43\text{GPa}, 3.91\text{GPa})$  with the  $\hat{\mathbf{w}}^{(0)}$ , while  $(C_{11}, C_{12}, C_{44}) = (9.40\text{GPa}, 3.02\text{GPa}, 3.26\text{GPa})$  with the modified  $\hat{\mathbf{w}}$ . They should be compared with  $(C_{11}, C_{12}, C_{44}) = (9.17\text{GPa}, 5.64\text{GPa}, 4.52\text{GPa})$  for the atomic system. The underestimation of  $C_{12}$  and  $C_{44}$  in the CGP method with the  $\hat{\mathbf{w}}^{(0)}$ , which is due to the introduction of the truncation to  $\mathbf{K}$ , has been pointed out for the Ar systems in 2D and 3D also. Separately we try to use  $\hat{\mathbf{w}}$  modified from  $\hat{\mathbf{w}}^{(0)} = (\hat{\mathbf{N}}\hat{\mathbf{N}}^T)^{-1}\hat{\mathbf{N}}$  with the Hermitian, non-linear- $\mathbf{N}$ . The calculated elastic moduli of the CGP system change little from the ones with the linear- $\mathbf{N}$ .

If we release the constraint in  $w_{I\mu,iv} = \hat{w}_{Ii}\delta_{\mu v}$  for the directional dependence, the CGP displacement in  $\mu$ -direction can be related to the atomic displacement in  $v$ -direction also. In the case, we may be able to optimize  $\mathbf{w}$  for the truncated  $\mathbf{K}$  to well reproduce all the three quantities of interest (the elastic moduli, the phonon dispersion relation, and the deformation energy). But it is not straightforward to find the proper directional-dependence of  $w_{I\mu,iv}$ . Therefore we conclude from the

point of simplicity that either  $\hat{\mathbf{w}}^{(0)} = (\hat{\mathbf{N}}\hat{\mathbf{N}}^T)^{-1}\hat{\mathbf{N}}$  with the linear- $\mathbf{N}$  or the modified  $\hat{\mathbf{w}}$  that reproduces well the deformation energy is a reasonable choice for 2D and 3D systems depending on our requirement.

#### 4 Anharmonicity at Finite Temperatures

A fundamental assumption in the former CGP method explained above is the harmonic approximation for the inter-atomic potential energy. Because of this, the former CGP method gives simply the ground-state energy of the atomic system for a given set of relatively small displacements of particles. Essentially no temperature effects are included. Therefore application of the former CGP method has been limited to a crystalline solid at low  $T$ 's. To overcome this, we improve the CGP method to use the inter-atomic potential directly at finite  $T$  without using the harmonic approximation, and thereby obtain the explicit dependencies of the inter-particle interaction on  $T$  and displacement.

When the temperature of a material in solid phase is raised, both thermal expansion and change in elasticity occur usually relating to the anharmonicity of the inter-atomic potential. We here incorporate those effects into the CGP system. The extent of the thermal expansion at a given  $T$  is evaluated by performing separately the MD simulation of the atomic system. As for the change in elasticity, we perform the Monte Carlo (MC) simulation to calculate the force on the CGP as follows.

Since the Helmholtz free-energy at a given  $\beta$  is  $G = -(1/\beta)\ln Z_{\text{CGP}}$ , the force acting on particle- $I$  in direction- $\mu$  is

$$F_{I\mu} = -\frac{\partial G}{\partial U_{I\mu}} = \frac{1}{\beta Z_{\text{CGP}}} \left( \prod_k^{N_{\text{atom}}} \iint d\mathbf{u}_k d\mathbf{p}_k \right) \exp(-\beta H_{\text{atom}}) \Delta \frac{\partial \Delta}{\partial U_{I\mu}}. \quad (21)$$

Exploiting the chain rule

$$\frac{\partial \Delta}{\partial U_{I\mu}} = \sum_i \frac{\partial u_{i\mu}}{\partial U_{I\mu}} \frac{\partial \Delta}{\partial u_{i\mu}}, \quad (22)$$

we obtain through the integral by parts as

$$\begin{aligned}
 F_{I\mu} &= \frac{1}{\beta Z_{CGP}} \left( \prod_k^{N_{atom}} \iint d\mathbf{u}_k d\mathbf{p}_k \right) \exp(-\beta H_{atom}) \dot{\Delta} \sum_i \frac{\partial u_{i\mu}}{\partial U_{I\mu}} \frac{\partial \Delta}{\partial u_{i\mu}} \\
 &= -\frac{1}{\beta Z_{CGP}} \left( \prod_k^{N_{atom}} \iint d\mathbf{u}_k d\mathbf{p}_k \right) \sum_i \frac{\partial \exp(-\beta H_{atom})}{\partial u_{i\mu}} \dot{\Delta} \frac{\partial u_{i\mu}}{\partial U_{I\mu}} \Delta \\
 &= \frac{1}{Z_{CGP}} \left( \prod_k^{N_{atom}} \iint d\mathbf{u}_k d\mathbf{p}_k \right) \sum_i \frac{\partial H_{atom}}{\partial u_{i\mu}} \exp(-\beta H_{atom}) \frac{\partial u_{i\mu}}{\partial U_{I\mu}} \dot{\Delta} \Delta \\
 &= - \left\langle \sum_i \frac{\partial u_{i\mu}}{\partial U_{I\mu}} f_{i\mu} \right\rangle_{\mathbf{U}=\mathbf{w}\mathbf{u}} . \tag{23}
 \end{aligned}$$

We note that the calculation of  $F_{I\mu}$  in this form requires the atomic ensemble for the partial differentiation  $\partial u_{i\mu}/\partial U_{I\mu}$  under the constraint  $\mathbf{U} = \mathbf{w}\mathbf{u}$ . The numerical evaluation of  $\partial u_{i\mu}/\partial U_{I\mu}$  for each atomic configuration that satisfies  $\mathbf{U} = \mathbf{w}\mathbf{u}$  is cumbersome. To overcome the difficulty, we exploit the relation

$$\begin{aligned}
 &- \left\langle \sum_i \frac{\partial u_{i\mu}}{\partial U_{I\mu}} f_{i\mu} \right\rangle_{\mathbf{U}=\mathbf{w}\mathbf{u}} \\
 = &- \left\langle \sum_i \frac{\partial (u_{i\mu} f_{i\mu})}{\partial U_{I\mu}} \right\rangle_{\mathbf{U}=\mathbf{w}\mathbf{u}} + \left\langle \sum_i \frac{\partial f_{i\mu}}{\partial U_{I\mu}} u_{i\mu} \right\rangle_{\mathbf{U}=\mathbf{w}\mathbf{u}} \tag{24}
 \end{aligned}$$

and ignore accurately the second term on the right hand side of Eq. (24) by displacing the origin of  $u_{i\mu}$  temporarily to  $\langle u_{i\mu} \rangle_{\mathbf{U}=\mathbf{w}\mathbf{u}}$ . We thereby obtain the formula

$$\begin{aligned}
 F_{I\mu} = &-\frac{1}{\Delta U_{I\mu}} \left[ \left\langle \sum_i (u_{i\mu} - \langle u_{i\mu} \rangle_{\mathbf{U}=\mathbf{w}\mathbf{u}}) f_{i\mu} \right\rangle_{\mathbf{U}+\Delta\mathbf{U}=\mathbf{w}\mathbf{u}} \right. \\
 &\left. - \left\langle \sum_i (u_{i\mu} - \langle u_{i\mu} \rangle_{\mathbf{U}=\mathbf{w}\mathbf{u}}) f_{i\mu} \right\rangle_{\mathbf{U}=\mathbf{w}\mathbf{u}} \right] \tag{25}
 \end{aligned}$$

with  $\mathbf{U} + \Delta\mathbf{U} = (\mathbf{U}_1, \mathbf{U}_2, \dots, \mathbf{U}_I + \Delta U_{I\mu}, \mathbf{U}_{I+1}, \dots)$ . As desired, the numerical evaluation of Eq. (25) requires two mutually independent sets of the atomic configurations: one for the constraint  $\mathbf{U} + \Delta\mathbf{U} = \mathbf{w}\mathbf{u}$  and the other for  $\mathbf{U} = \mathbf{w}\mathbf{u}$ . The possible  $T$ -dependence of  $\mathbf{w}$  is ignored and  $\hat{\mathbf{w}} = \hat{\mathbf{w}}^{(0)} \equiv (\hat{\mathbf{N}}\hat{\mathbf{N}}^T)^{-1}\hat{\mathbf{N}}$  with the linear- $\mathbf{N}$ .

We calculate the forces  $\mathbf{F}$  on the particles at given  $T$ 's by the MC method with the Metropolis algorithm[e.g., Allen and Tildesley (1987)] for a given set of the particle displacements  $\mathbf{U}$ . The force components,  $\{F_{I\mu}\}$ , can be computed in parallel. As

demonstrations, we consider two different types of atomic systems in both 1D and 2D: one is the Ar crystal with the LJ potential and the other is the Al crystal with the EAM potential (*i.e.*, a multi-body type). Under the PBC's, the atoms are set initially at equal spacing in 1D; the atoms are set to form the triangular lattice in 2D. The  $r_{CG} = 10$  for 1D and 18 for 2D. In each MC run, the size of the simulation box is set to realize essentially zero-stress (or pressure) situation by referring to the pre-computed thermal expansion rates. We here define  $a_{\text{atom}}$  as the averaged inter-atomic spacing that depends on  $T$ . The  $a_{\text{atom}} = 3.75\text{\AA}$ (1D-Ar),  $2.38\text{\AA}$ (1D-Al),  $3.74\text{\AA}$ (2D-Ar),  $2.67\text{\AA}$ (2D-Al) at  $T \ll 1\text{K}$ . The linear thermal expansion rates per Kelvin of  $a_{\text{atom}}$  for the Al systems are  $1.53 \times 10^{-4} \text{K}^{-1}$  for 1D and  $2.7 \times 10^{-4} \text{K}^{-1}$  for 2D; the same thermal expansion rates are applied to the Ar system for better comparison of the Ar and Al systems. The numbers of atoms in the MC runs are large enough to calculate the forces on particles. About  $10^3$  trials per atom are needed for accurate MC sampling of  $F_{Ix}$  with the acceptance ratio of about 50%.

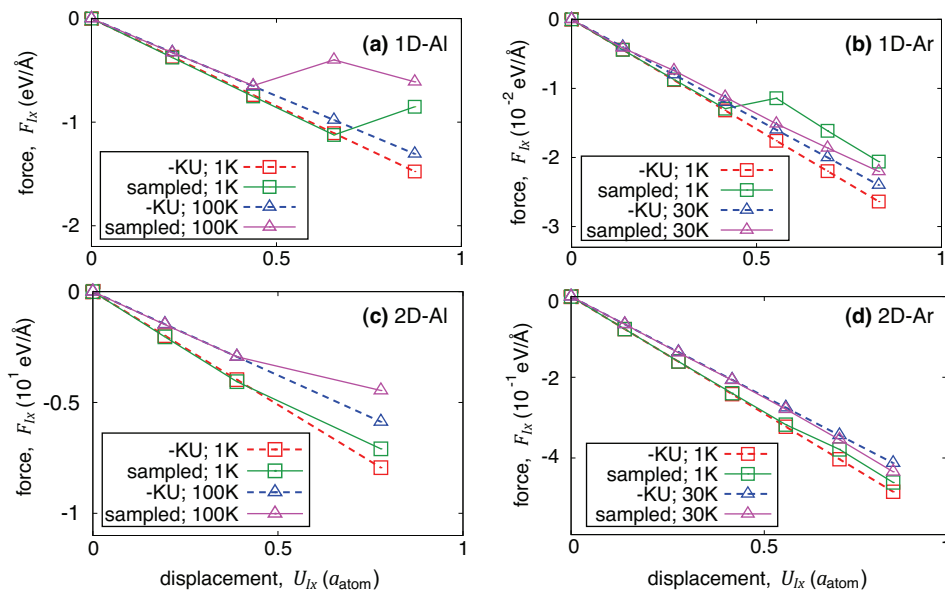


Figure 4: The Monte Carlo sampling results for the force  $F_{Ix}$  on particle- $I$  when it is displaced by  $U_{Ix}$ . The  $r_{CG} = 10$  for 1D and 18 for 2D. For a reference,  $F_{Ix} = -K_{Ix,Ix}U_{Ix}$  is plotted with  $K_{Ix,Ix}$  calculated by applying the harmonic approximation to the inter-atomic potential with the thermal expansion incorporated. (a) for 1D-Al, (b) For 1D-Ar, (c) for 2D-Al, and (d) for 2D-Ar.

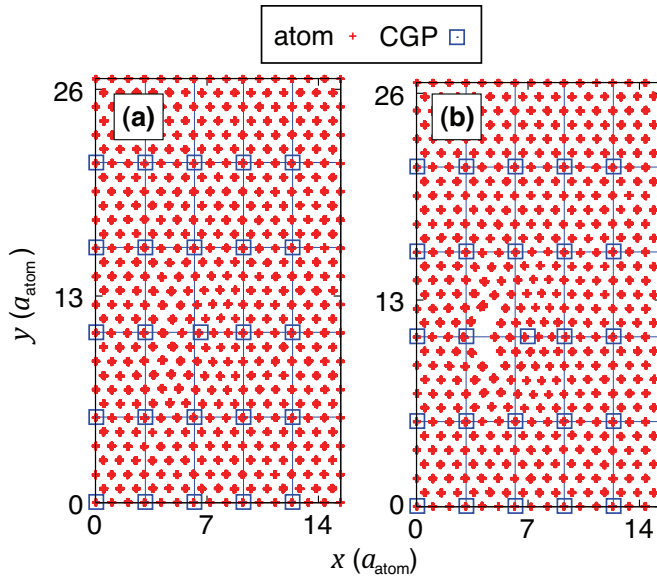


Figure 5: The accumulated positions of the atoms in the Monte Carlo sampling for the given configuration of CGP's. The system is 2D-Al at  $T = 100\text{K}$  with  $r_{CG} = 18$ . The grid is drawn for the guide to the eyes. (a) for  $U_{Ix} = 0.38a_{\text{atom}}$ . (b) for  $U_{Ix} = 0.77a_{\text{atom}}$ .

Figure 4 shows the calculated values of  $F_{Ix}$  as a function of the displacement  $U_{Ix} (> 0)$ , while the other particles ( $\neq I$ ) are fixed: (a) for 1D-Al, (b) for 1D-Ar, (c) for 2D-Al, and (d) for 2D-Ar. The possible error in the MC sampling in each panel in Fig. 4 is as small as the line width. For references, the values of  $F_{Ix} = -K_{Ix,Ix}U_{Ix}$  are plotted, where  $K_{Ix,Ix}$  is calculated by applying the harmonic approximation to the inter-atomic potential with the thermal expansion incorporated. We find in Fig. 4 that: (i) In all four case,  $F_{Ix}$  is linear in  $U_{Ix}$  at  $U_{Ix} < 0.4a_{\text{atom}}$  at both low and high  $T$ 's. The  $F_{Ix}$  in the linear regime compares quite well with that in the harmonic approximation; (ii) Deviation of  $F_{Ix}$  from the linear behavior is significant at large  $U_{Ix}$  in both Ar and Al systems irrespective of  $T$ . We here add that if the Brenner inter-atomic potential [Brenner (1990)] is used to describe a graphene sheet (*i.e.*, 2D system) a smooth non-linear softening is observed in the CGP system with  $r_{CG} = 4$  for  $U_{Ix} > 0.2a_{\text{atom}}$  with  $a_{\text{atom}} = 1.53\text{\AA}$ .

Figure 5 depicts the accumulated atomic positions of the 2D-Al system at  $T = 100\text{K}$  in the MC sampling relating to the positions of CGP's with (a)  $U_{Ix} = 0.38a_{\text{atom}}$  or (b)  $U_{Ix} = 0.77a_{\text{atom}}$ . As expected, the MC-averaged positions of those atoms near

particle- $I$  that is displaced to  $x$ -direction shift to the same direction. In the case of  $U_{Ix} = 0.38a_{\text{atom}}$ , the Al atoms vibrate thermally under the constraint  $\mathbf{U} = \mathbf{w}\mathbf{u}$  forming a deformed lattice. The atomic lattice is broken in the case of  $U_{Ix} = 0.77a_{\text{atom}}$  due to its largeness. It means that one must be careful in applying the CGP method directly to those problems where local deformation can be large. However, the situation of large local-deformation to such an extent that the atomic lattice breaks is not expected particularly for large  $r_{\text{CG}}$  since a CGP represents a large group of atoms.

As for the apparent linear behavior of  $F_{Ix}$  as a function of  $U_{Ix}$  in the Ar and Al systems (see, Fig. 4), one might imagine much pronounced non-linear behavior considering the highly non-linear nature of the inter-atomic potential. To understand the reason of our finding, we perform separately a test calculation to calculate the force  $f_{ix}$  when only atom- $i$  is displaced by  $u_{ix}$  from the crystalline Al described by the EAM potential at the ground state, which corresponds to  $r_{\text{CG}} = 1$ . We in fact find a linear dependence of  $f_{ix}$  on  $u_{ix}$  by mutual cancellation of the non-linearity in force from the expansion and compression regions; a non-linear softening is observed if  $u_{ix} > 0.35a_{\text{atom}}$ . Such a canceling mechanism works also for the coarse-grained system.

The MC sampling results of  $F_{Ix}$  explained above is for the case in which a single CGP is displaced by  $U_{I\mu}$  with the others fixed. The observed linear-behavior may be written as  $F_{I\mu} = -K_{I\mu,I\mu}(T)U_{I\mu}$  using the  $T$ -dependent stiffness-element  $K_{I\mu,I\mu}(T)$ . The  $K_{I\mu,I\mu}(T)$  compares quite well with that calculated by applying the harmonic approximation to the inter-atomic potential with the thermal expansion incorporated. When two CGP's ( $I$  and  $J$ ) are displaced together by  $U_{I\mu}$  and  $U_{J\nu}$  with the others fixed, we may obtain another stiffness-element  $K_{I\mu,J\nu}(T)$  in  $F_{I\mu} = -K_{I\mu,I\mu}(T)U_{I\mu} - K_{I\mu,J\nu}(T)U_{J\nu}$  through  $U_{J\nu}$ -dependence of  $F_{I\mu}$ . We thereby find that the  $K_{I\mu,J\nu}(T)$  compares also well with that calculated for the thermally expanded system of atoms with the harmonic approximation. Since the MC sampling can be performed with any desired boundary condition, the present MC method can be applied to evaluate  $\mathbf{K}$  for inhomogeneous systems as surface, to which Eq. (10) that assumes the PBC's cannot be applied.

We here remark that Ref. [Curtarolo and Ceder (2002)] proposed an interesting approach to obtain the partition function of a uniformly coarse-grained system, by performing the phase-space integrations of the atomic partition function in a recursive manner using the Migdal-Kadanoff approximation in the renormalization group theory. Their approach is similar to the CGP method, but differs in using a different mathematical method to perform approximately the constrained phase-space integrations of the atomic partition function. Reference [Dupuy, Tadmor, Miller, and Phillips (2005)] proposed a simple method, based on Ref. [Shenoy,

Shenoy, and Phillips (1999)], to take into account the harmonic oscillation of atoms at finite temperatures in the QC method. However, the method ignores both anharmonicity of the inter-atomic potential and collective motion of atoms.

## 5 Demonstrative Applications

### 5.1 Wave propagation in anharmonic solid

In the preceding section, we have found that the force on a CGP shows a linear dependence on the displacement for both Ar and Al systems when the displacement (or deformation) is not too large to break the crystalline structure. Also the force on a CGP at finite temperature is well described through the dynamical matrix of the atomic system in the harmonic approximation with the specific-volume change incorporated. We exploit these findings to get the potential energy and the forces for a given configuration of CGP's in a simple way. We denote  $\Omega_0$  as the specific-volume and  $R_{IJ}^{(0)}(\Omega_0)$  as the equilibrium distance at the equilibrium volume ( $T = 0$ ). For each stiffness-element  $K_{IJ}$  (the direction index is omitted for simplicity), (i) firstly we calculate  $\{K_{IJ}(\Omega_m)\}$  with Eq. (10) at various specific-volumes  $\{\Omega_m\}$  ( $m = 0, \pm 1, \pm 2, \dots$ ), (ii) secondary we prepare to interpolate  $\{K_{IJ}(\Omega_m)\}$  in order to evaluate  $K_{IJ}(\Omega)$  at any  $\Omega$  around particles- $I$  and  $J$ , and (iii) finally considering the relation of  $R_{IJ}$  to  $\Omega$  we integrate  $K_{IJ}(\Omega)$  by  $R_{IJ}$  to get the corresponding force and potential energy (*i.e.*, free energy) at the present  $\Omega$ .

Denoting  $\tilde{V}_{CGP}(R_{IJ})$  as the potential-energy term involving  $R_{IJ}$  at  $\Omega$  with  $\Omega_m < \Omega < \Omega_{m+1}$ , we evaluate  $K_{IJ}(\Omega) = -\tilde{V}_{CGP}''(R_{IJ}) \equiv -(d^2/dR_{IJ}^2)\tilde{V}_{CGP}(R_{IJ})$  by interpolating  $\{K_{IJ}(\Omega_m)\}$  linearly in the  $\Omega$ -segment:

$$K_{IJ}(\Omega) = \frac{1}{R_{IJ}^{(0)}(\Omega_{m+1}) - R_{IJ}^{(0)}(\Omega_m)} \times \left[ K_{IJ}(\Omega_{m+1})\{R_{IJ} - R_{IJ}^{(0)}(\Omega_m)\} + K_{IJ}(\Omega_m)\{R_{IJ}^{(0)}(\Omega_{m+1}) - R_{IJ}\} \right]. \quad (26)$$

Integration of  $K_{IJ}(\Omega)$  by  $R_{IJ}$  from  $R_{IJ}^{(0)}(\Omega_0)$  until the present  $R_{IJ}$  spanning  $\Omega$ -segments gives

$$\tilde{V}'_{CGP}(R_{IJ}) = - \int_{R_{IJ}^{(0)}(\Omega_0)}^{R_{IJ}} K_{IJ}(\Omega) dR \quad (27)$$

and

$$\tilde{V}_{CGP}(R_{IJ}) = \int_{R_{IJ}^{(0)}(\Omega_0)}^{R_{IJ}} \tilde{V}'_{CGP}(R) dR. \quad (28)$$

In the integrations we have used  $\tilde{V}'_{\text{CGP}}(R_{IJ}^{(0)}(\Omega_0)) = 0$  from the definition of  $\Omega_0$  and  $\tilde{V}_{\text{CGP}}(R_{IJ}^{(0)}(\Omega_0)) = 0$  as the basis of the potential energy. As a result,  $\tilde{V}_{\text{CGP}}(R_{IJ})$  becomes a cubic polynomial of  $R_{IJ}$  for each  $\Omega$ -segment. In the present application, Eq. (26) is applied to each particle pair ( $I$  and  $J$ ) by regarding  $R_{IJ}$  as  $\Omega$ .

To check the physical accuracy of the present representation of  $\tilde{V}_{\text{CGP}}(R_{IJ})$ , we consider the behavior of wave propagation in the 1D-Ar system under the PBC interacting with the LJ potential. We compare the full-atom MD and the CGP dynamics with  $r_{\text{CG}} = 10$ . The optimized weight-matrix,  $\mathbf{w}$ , obtained by starting from  $\mathbf{w}^{(0)}$  with the linear- $\mathbf{N}$ , is used to calculate the stiffness matrix  $\mathbf{K}_{IJ}$ . A Gaussian-form, longitudinal displacement field is applied to the system with zero initial velocity, as shown in Fig. 6(a). Relating to largeness of the amplitude of the wave (initially,  $6a_{\text{atom}}$ ), the specific volume varies initially by 5% at the largest. For the CGP dynamics, interpolation of  $K_{IJ}(\Omega_m)$  is performed at either every 1%- or 8%-change of  $\Omega$ . The CGP dynamics without interpolation, which corresponds to the former CGP method, is also performed for reference. Figures 6(b)-(d) show the time-evolution of the wave.

As we observe for the MD results in Figs. 6(b) and 6(c), the decompression wave moving to the left has a spiky displacement-field, while the compression wave moving to the right a smooth one. Such a difference is described correctly by the CGP method with both 1%- and 8%-interpolations. At the collision of the two waves in Fig. 6(d), the CGP dynamics with 1%-interpolation corresponds quite well to the MD. Even with 8%-interpolation, we find the CGP dynamics become better than the case without interpolation. We may state that the CGP simulation with the present stiffness-interpolation method successfully takes into account the anharmonicity of the original atomic system at finite temperatures.

## 5.2 Wave scattering by point defect

As another test system, we prepare a graphene sheet of size  $97.2\text{\AA} \times 168.86\text{\AA}$  under the PBC's with a single C atom removed to form a single-atom vacancy. The Brenner inter-atomic potential [Brenner (1990)] is used for the atomic system. Two characteristic regions are considered to apply the coarse graining procedure with  $r_{\text{CG}} = 4$ . The one includes the vacancy, while the other is in the bulk phase. Figure 7 depicts the arrangement of the C atoms (the circles) and the CG particles (the squares) to calculate  $\mathbf{K}$  for the region with the vacancy. The hatched region corresponds to the unit cell of the CGP system. For the weight matrix,  $\hat{\mathbf{w}}^{(0)}$  with the linear- $\mathbf{N}$  is used for both regions. We are interested in the situation of low temperatures. In the situation, the MC sampling of atoms  $\langle \dots \rangle_{\mathbf{U}=\mathbf{w}\mathbf{u}}$  in Eq. (25) corresponds to finding the fully relaxed configuration of atoms under the constraint  $\mathbf{U} = \mathbf{w}\mathbf{u}$ . To investigate the accuracy of the CGP method when it is applied to such an inhomoge-

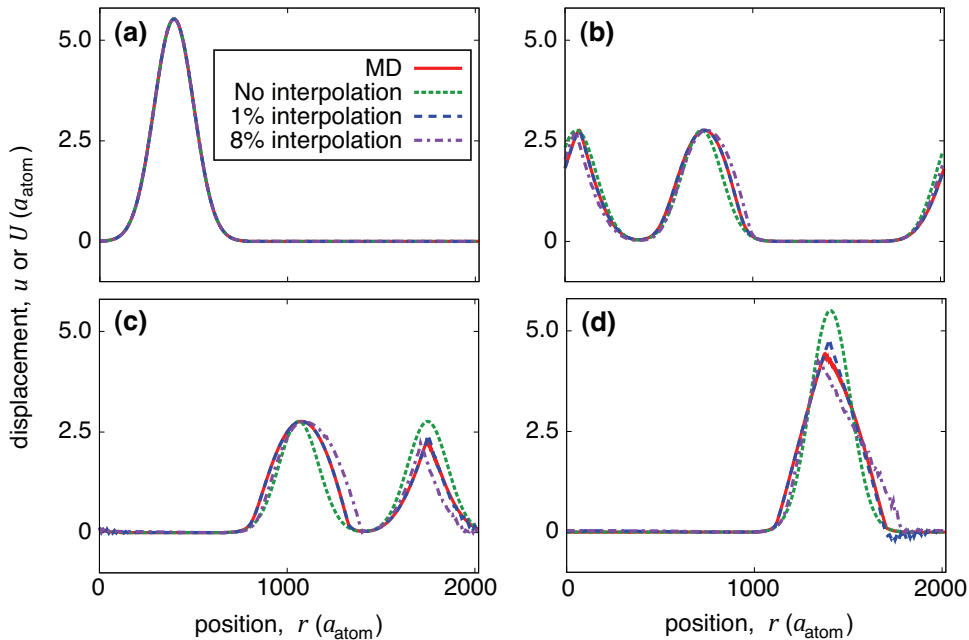


Figure 6: The propagation of longitudinal wave in the 1D-Ar system with  $a_{\text{atom}} = 3.75\text{\AA}$ . The MD means the full-atom simulation. The stiffness matrix in the CGP method with  $r_{\text{CG}} = 10$  is interpolated between the pre-computed values at every 1% or 8%-change of the specific-volume. (a) at  $t = 0\text{ps}$ , (b) at  $t = 96.7\text{ps}$ , (c) at  $t = 193.4\text{ps}$ , and (d) at  $t = 290.1\text{ps}$ .

neous system with a vacancy, we compare the deformation field formed around the vacancy. Figure 8 compares (a) the deformation field in  $x$ -direction obtained with the MD (or full-atom) method and (b) the one with the CGP method. Both shape and intensity of the field are reproduced well with the CGP method. Incorrectness on several points at close proximity to the vacancy in Fig. 8(b) originates from our simple arrangement of the CG particles. In fact, it can be corrected substantially if the CG particles are arranged to match with the rotational symmetry of the graphene system without a vacancy. However we consider that the simple arrangement of the CG particles is satisfactory for many processes relating to the waves with the wavelengths much larger than the inter-particle spacing.

Table 1 compares the calculated values of the stiffness-matrix  $\mathbf{K}_{12}$  for the neighboring particles between the region with the vacancy and the region without it (*i.e.*, the perfect graphene). The  $\mathbf{K}_{1y,2y}$  is modified substantially by the vacancy.

Table 1: Calculated values of the stiffness matrix  $\mathbf{K}_{12}$  (see, Fig. 7 for the definition of particles 1 and 2) in the coarse-grained graphene system with a single-atom vacancy. For references, corresponding values without vacancy (*i.e.*, perfect crystal) are given.

	$K_{1x2x}$ (GPa)	$K_{1x2y}$ (GPa)	$K_{1y2y}$ (GPa)	$K_{1z2z}$ (GPa)
with vacancy	-134.36	-6.29	-60.27	-18.61
without vacancy	-123.48	-9.20	-12.44	-14.52

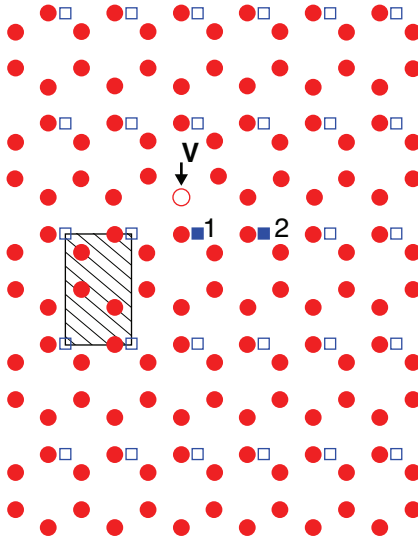


Figure 7: A region of the graphene around a vacancy, which is used to calculate the stiffness matrix between the neighboring particles 1 and 2. The filled circles are the C atoms, while the squares represent the particles. The open circle indicated by the arrow is the vacancy site. The hatched region is the unit cell of the CGP system that includes 4 atoms and 1 particle (*i.e.*,  $r_{CG} = 4$ ).

Note that  $\mathbf{K}_{12}$  is for a neighboring particle pair and therefore takes on minus values. To demonstrate successful incorporation of the vacancy in the CGP method through the stiffness-matrix, we simulate the wave scattering by the vacancy in graphene. Initially we shift the peripheral atoms or particles at lower- $y$  area of  $y$ -width  $21.04\text{\AA}$  to  $y$ -direction sinusoidally (the phase width  $2\pi$  radian and the amplitude  $0.156\text{\AA}$ ). The oscillatory wave propagates and then scatters around the va-

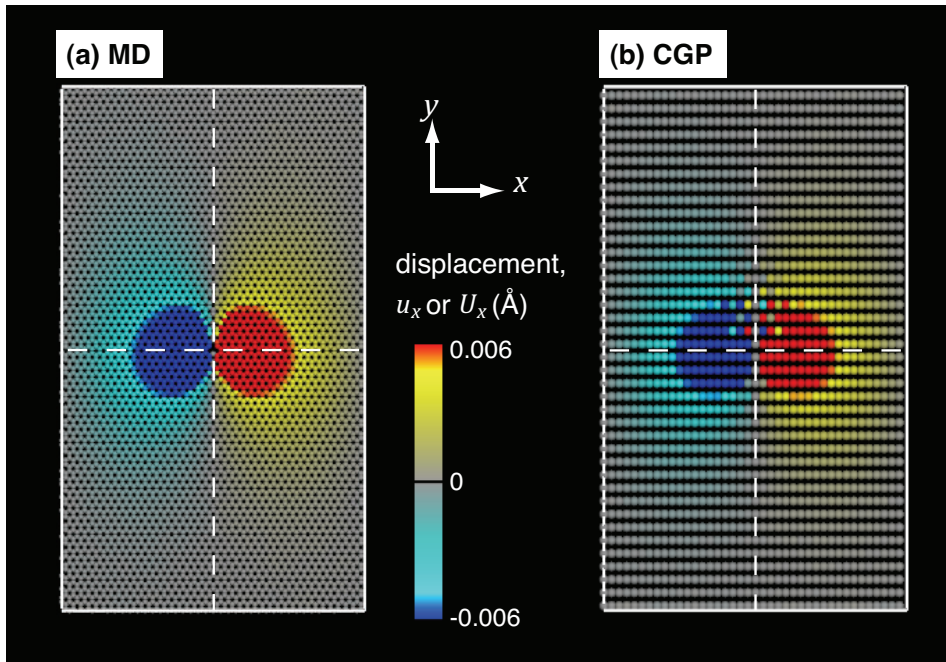


Figure 8: The initial displacement field in  $x$ -direction in the graphene with a vacancy. (a) for the full-atom simulation result. (b) for the CGP result with  $r_{CG} = 4$ . Dashed lines are drawn for the guide.

cancy. Figure 9 compares the snapshots of the wave scattering between the MD and CGP systems at 259.2fs after the wave front reached the vacancy site. We observe in Fig. 9(b) that the mirror symmetry with respect to the vertical dashed-line exists to some extent in the CGP system as the initial strain field in Fig. 8(b). In the lower- $y$  half region of Fig. 9(b), the peak positions of the displacement field in the CGP system correspond well to that in the MD system. However, in the upper half region, we observe substantial weakening of the intensity of the displacement in comparison to the MD results. We guess that the rather unsmooth deformation observed at several points in the upper half region of Fig. 8(b) worked to create artificial scattering waves, resulting in such a weakening of the intensity.

The single-atom vacancy in the present setting may be regarded as one of the most stringent test system for the coarse graining schemes. Slight difference in the scattering behavior seen in Fig. 9, demonstrates the inaccuracy of the coarse graining in such an extreme situation. If the target atomic system with a point defect are coarse-grained uniformly to a higher degree, the effect of the point defect will be

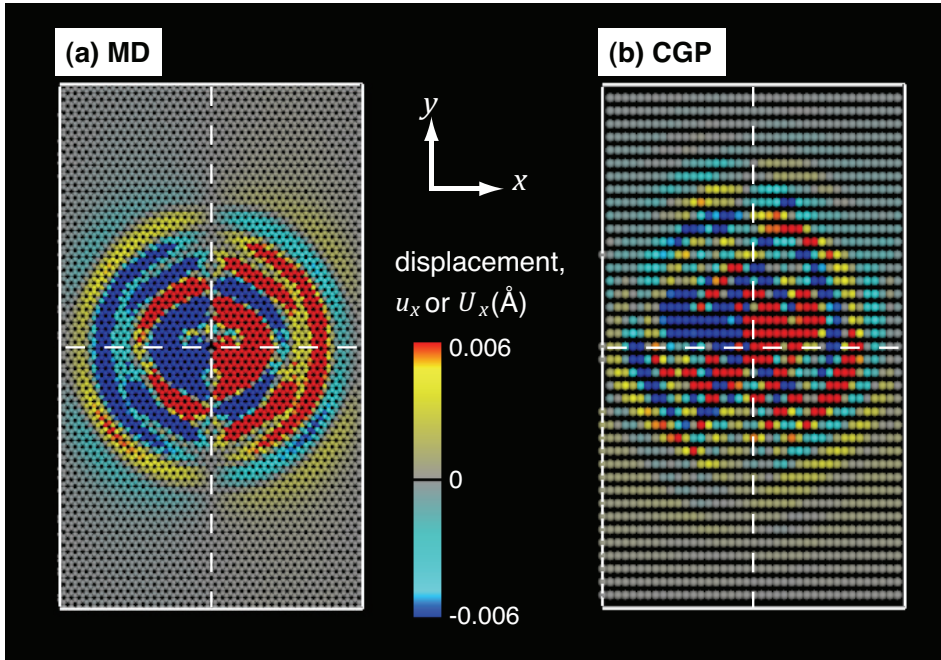


Figure 9: The snapshots of displacement field in  $x$ -direction at 259.2fs after the wave front reached the vacancy in the graphene. (a) for the full-atom simulation result. (b) for the CGP result with  $r_{CG} = 4$ . Dashed lines are drawn for the guide.

smoothed away substantially due to the nature of coarse graining. In such a situation, a lower degree of the coarse graining or even the MD method should be applied at around the point defect. Considering these, we are presently working to couple such regions with different coarse-graining degrees.

## 6 Summary and Concluding Remarks

In this paper we have improved the former CGP method in the following three points. Firstly, the weight matrix ( $\mathbf{w}$ ) that is used in averaging the atomic displacements to obtain the particle ones, has been determined to reproduce together the phonon dispersion relation, the elastic moduli, and the deformation energies at various wavenumbers. For 1D systems we have found that the deformation energies at relatively large wavenumbers are corrected well while the phonon dispersion relation and the elastic constant are reproduced accurately by using the optimized  $\mathbf{w}$ . For 2D and 3D systems, on the other hand, we could not have found signifi-

cant improvement from the case of using  $\mathbf{w}^{(0)}$  with the linear- $\mathbf{N}$  in the search for proper  $\mathbf{w}$ . Secondary, we have developed the MC sampling method to incorporate from the first principles the anharmonicity of atomic system at finite temperatures into the particle force. The MC results have shown that the inter-particle interaction energy is reproduced well in the harmonic form with the change in the local specific-volume due to thermal expansion incorporated properly. Thirdly, we have proposed the divide-and-conquer approach to evaluate the inter-particle interaction for each region in an inhomogeneous system.

To confirm increased accuracy of the improved CGP method for various phenomena, we have simulated the longitudinal wave-propagation with large initial amplitude. We have used the stiffness-interpolation method to take into account the anharmonicity of the atomic system at finite temperatures. We then have found high reproductivity of the improved CGP method including the spiky profile of the decompression wave, which cannot be describe with the former CGP method. Another application of the improved CGP method to the graphene sheet with a vacancy has demonstrated its reasonable reproductivity of both deformation field and wave scattering caused by the vacancy.

In our search for proper  $\mathbf{w}$ , we could not have corrected the shear moduli ( $C_{12}$  and  $C_{44}$ ) of the 3D-Al system calculated with the present CGP method (see, Sec. 4). When we apply the CGP method to real problems in 2D or 3D, we may take a different idea to correct them. If we perform eigen-mode analyses for  $\mathbf{K}$  and modify the eigen-values of selected eigen-modes, we find all the elastic moduli reproduced accurately without affecting the phonon dispersion relation and the deformation energies at various wavenumbers. Details of the idea will be explained in a separate paper.

## References

- Allen, M. P.; Tildesley, D.** (1987): *Computer simulation of liquids*. Clarendon, Oxford.
- Anderson, T. L.** (1995): *Fracture mechanics, 2nd ed.* CRC Press, N.Y.
- Ashcroft, N. W.; Mermin, N. D.** (1976): *Solid state physics*. HRW Int'l ed. (Saunders College, Philadelphia).
- Brenner, D. W.** (1990): Empirical potential for hydrocarbons for use in simulating the chemical vapor deposition of diamond films. *Phys. Rev. B*, vol. 42, pp. 9458–9471.
- Broughton, J. Q.; Abraham, F. F.; Bernstein, N.; Kaxiras, E.** (1999): Concurrent coupling of length scales: Methodology and application. *Phys. Rev. B*, vol. 60, pp. 2391–2403.

- Cook, R. D. Malkus, D. S.; Plesh, M. E.** (1989): *Concepts and applications of finite element analysis, 3rd ed.* Wiley, NY.
- Curtarolo, S.; Ceder, G.** (2002): Dynamics of an inhomogeneously coarse grained multiscale system. *Phys. Rev. Lett.*, vol. 88, pp. 255504–(1–4).
- Curtin, W. A.; Miller, R. E.** (2003): Atomistic/continuum coupling in computational materials science. *Modeling Simul. Mater. Sci Eng.*, vol. 11, pp. R33–R68.
- Dapprich, S.; Komáromi, I.; Byun, K. S.; Morokuma, K.; Frisch, M. J.** (1999): A new oniom implementation in gaussian98. part i. the calculation of energies, gradients, vibrational frequencies and electric field derivatives. *J. Mol. Struct. (Theochem)*, vol. 461–462, pp. 1–21.
- Dupuy, L. M.; Tadmor, E. B.; Miller, R. E.; Phillips, R.** (2005): Finite-temperature quasicontinuum: Molecular dynamics without all the atoms. *Phys. Rev. Lett.*, vol. 95, no. 6, pp. 060202–(1–4).
- Fendler, J. H.** (1998): *Nanoparticles and nanostructured films.* Wiley-VCH, NY.
- Finnis, M. W.; Sinclair, J. E.** (1984): A simple empirical N-body potential for transition metals. *Phil. Mag. A*, vol. 50, pp. 45–55.
- Gad-el-Hak, M.** (2001): *The MEMS Handbook.* CRC Press.
- Kakiras, E.** (2003): *Atomic and Electronic Structure of Solids.* Cambridge Univ. Press, New York.
- Kobayashi, R.; Nakamura, T.; Ogata, S.** (2008): Development and implementation of recursive coarse-grained particle method for meso-scale simulation. *Materials transactions*, vol. 49, pp. 2541–2549.
- Kobayashi, R.; Nakamura, T.; Ogata, S.** (2010): A simple dynamical scale-coupling method for concurrent simulation of hybridized atomistic/coarse-grained-particle system. *Inter. J. Num. Meth. Eng.*, vol. 83, pp. 249–268.
- Liu, W. K.; Karpov, E. G.; Zhang, S.; Park, H. S.** (2004): An introduction to computational nanomechanics and materials. *Comput. Meth. Appl. Mech. Eng.*, vol. 193, pp. 1529–1578.
- Lu, G.; Kakiras, E.** (2005): Overview of multiscale simulation of materials. *Handbook of theoretical and computational nanotechnology*, vol. X chap. 22.
- Miller, R. E.; Tadmor, E. B.** (2002): The Quasicontinuum Method: Overview, applications and current directions. *Journal of Computer-Aided Materials Design*, vol. 9, pp. 203–239.
- Mullins, M.; Dokainish, M. A.** (1982): Simulation of the (001) plane crack in  $\alpha$ -iron employing a new boundary scheme. *Phil. Mag. A*, vol. 46, pp. 771–787.

**Nakano, A.; Bachlechner, M. E.; Branicio, P.; Campbell, T. J.; Ebbsjo, I.; Kalia, R. K.; Madhukar, A.; Ogata, S.; Omeltchenko, A.; Rino, J. P.; Shimojo, F.; Walsh, P.; Vashishta, P.** (2000): Large-scale atomistic modeling of nanoelectronic structures. *IEEE Trans. Electr. Dev.*, vol. 47, pp. 1804–1810.

**Ogata, S.** (2005): Buffered-cluster method for hybridization of density-functional theory and classical molecular dynamics: Application to stress-dependent reaction of  $h_2o$  on nanostructured si. *Phys. Rev. B*, vol. 72, pp. 045348–045364.

**Ogata, S.; Abe, Y.; Ohba, N.; Kobayashi, R.** (2010): Stress-induced nano-oxidation of silicon by diamond-tip in moisture environment: A hybrid quantum-classical simulation study. *J. Appl. Phys.*, vol. 108, pp. 064313–(1–12).

**Ogata, S.; Lidorikis, E.; Shimojo, F.; Nakano, A.; Vashishta, P.; Kalia, R. K.** (2001): Hybrid finite-element/molecular-dynamics/electronic-density-functional approach to materials simulations on parallel computers. *Comp. Phys. Comm.*, vol. 138, pp. 143–154.

**Ogata, S.; Shimojo, F.; Kalia, R. K.; Nakano, A.; Vashishta, P.** (2002): Hybrid quantum mechanical/molecular dynamics simulation on parallel computers: density functional theory on real-space multigrids. *Comp. Phys. Comm.*, vol. 149, pp. 30–38.

**Rudd, R. E.; Broughton, J. Q.** (1998): Coarse-grained molecular dynamics and the atomic limit of finite elements. *Phys. Rev. B*, vol. 58, pp. R5893–R5896.

**Rudd, R. E.; Broughton, J. Q.** (2005): Coarse-grained molecular dynamics: Nonlinear finite elements and finite temperature. *Phys. Rev. B*, vol. 72, pp. 144104–(1–32).

**Sánchez-Portal, D.; Artacho, E.; Soler, J. M.** (1996): Analysis of atomic orbital basis sets from the projection of plane-wave results. *J. Phys.: Condens. Matter*, vol. 8, pp. 3859–3880.

**Shenoy, V.; Shenoy, V.; Phillips, R.** (1999): Finite temperature quasicontinuum methods. *Mater. Res. Soc. Symp. Proc.*, vol. 538, pp. 465–471.

**Smirnova, J. A.; Zhigilei, L. V.; Garrison, B. J.** (1999): A combined molecular dynamics and finite element method technique applied to laser induced pressure wave propagation. *Comp. Phys. Comm.*, vol. 118, pp. 11–16.

**Streitz, F. H.; Mintmire, J. W.** (1994): Electrostatic potentials for metal-oxide surfaces and interfaces. *Phys. Rev. B*, vol. 50, pp. 11996–12003.

**Tadmor, E. B.; Ortiz, M.; Phillips, R.** (1996): Quasicontinuum analysis of defects in solids. *Phil. Mag. A*, vol. 73, pp. 1529–1563.

**Tang, S.** (2008): A finite difference approach with velocity interfacial conditions for multiscale computations of crystalline solids. *J. Comp. Phys*, vol. 227, pp. 4038–4062.

**To, A. C.; Li, S.** (2005): Perfectly matched multiscale simulations. *Phys. Rev. B*, vol. 72, pp. 035414–(1–8).

**Xu, M.; Belytschko, T.** (2008): Conservation properties of the bridging domain method for coupled molecular/continuum dynamics. *Inter. J. Num. Meth. Eng.*, vol. 76, pp. 278–294.

